

Application of data assimilation methods to a dynamo model with turbulent magnetic helicity

By I. N. Kitiashvili, A. G. Kosovichev[†], T. Bewley[‡], J. Cessna[‡]
AND C. Colburn[‡]

1. Motivation and objectives

A thoughtful investigation of a natural phenomenon consists of three basic parts: observation, construction of a model and prediction. Predictions based on a model determine correctness of our understanding of the physical processes. Taking into account that observation data contain errors, and a model constructed on their basis is characterized by some approximations, a prediction of the next set of observations will deviate from the real data. Nevertheless, an estimate of uncertainties in the model and the observations allows us to correct the model solution according to the information obtained from new measurements. Thus, updated observation data and a consistent correction of the model solution allow us to improve the simulation results to more accurately describe the system's behavior and forecast its future state. This procedure also provides additional information for processes that are difficult to observe directly.

In this paper, we discuss initial results of applying the Ensemble Kalman Filter method (EnKF) to a simple non-linear dynamo model for analysis of the solar activity (Kitiashvili & Kosovichev 2008, 2009). One of the manifestations of solar magnetic activity is the 11-year sunspot cycle (Fig. 1a), which is characterized by fast growth and slow decay of the sunspot number parameter (Fig. 1b). For modeling the solar cycle we use a non-linear MHD dynamo model by Kleorin & Ruzmaikin (1982), which takes into account the dynamics of the turbulent magnetic helicity.

Many different data assimilation methods exist. Recently, hybrid methods based on a combination of other, simpler methods have emerged. For example, Ensemble Variational Estimation (EnVE) is a hybrid method of Ensemble Kalman Filter and 4D Variational (4DVar) methods. This method builds a better estimate state of the system, initial conditions and has a justifiable computational cost (Cessna *et al.* 2008; Bewley *et al.* 2008). Possibilities of the EnVE method application to dynamo models also will be discussed.

2. Formulation of the dynamo models

2.1. Parker's migratory dynamo

In a kinematic approximation, the dynamo problem can be described by the induction equation (Parker 1955)

$$\frac{\partial \mathbf{B}}{\partial t} = \nabla \times (\mathbf{v} \times \mathbf{B}) - \eta_m \nabla^2 \mathbf{B}, \quad (2.1)$$

where \mathbf{B} is the magnetic field strength, \mathbf{v} is the fluid velocity, η_m is the molecular magnetic diffusivity. Magnetic field, \mathbf{B} , and the fluid velocity, \mathbf{v} , can be separated into two

[†] W. W. Hansen Experimental Physics Laboratory, Stanford University, CA 94305, USA

[‡] Flow Control and Coordinated Robotics Labs, UC San Diego, CA 92093, USA

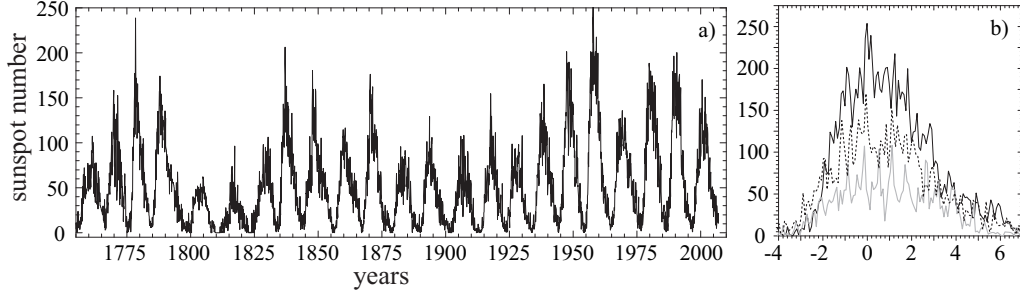


FIGURE 1. Observed monthly sunspot number series a) for 1755 – 2007 years from NGDC, and b) for three solar cycles 14 (gray curve), 19 (black curve) and 23 (dotted curve), which are aligned according to their maxima ($t = 0$).

components representing mean and fluctuating (turbulent) parts, or $\mathbf{B} = \langle \mathbf{B} \rangle + \mathbf{b}$ and $\mathbf{v} = \langle \mathbf{v} \rangle + \mathbf{u}$. Here, $\langle \mathbf{B} \rangle$ represents the longitudinally averaged magnetic field, \mathbf{b} is the fluctuating part of \mathbf{B} , $\langle \mathbf{v} \rangle$ represents mean global-scale motions in the Sun (such as the differential rotation), and \mathbf{u} is the velocity of turbulent convective motions. Taking into account that the average of fluctuations is zero, $\langle \mathbf{b} \rangle = \mathbf{0}$ and $\langle \mathbf{u} \rangle = \mathbf{0}$, for the case of isotropic turbulence, we obtain the following mean-field induction equation (e.g., Moffatt 1978)

$$\frac{\partial \langle \mathbf{B} \rangle}{\partial t} = \nabla \times (\langle \mathbf{v} \rangle \times \langle \mathbf{B} \rangle + \alpha \langle \mathbf{B} \rangle - \eta \nabla \times \langle \mathbf{B} \rangle), \quad (2.2)$$

where η describes the total magnetic diffusion, which is the sum of the turbulent and molecular magnetic diffusivity, $\eta = \eta_t + \eta_m$ (usually $\eta_m \ll \eta_t$). Parameter α is turbulent fluid helicity. The first term of the equation describes transport of magnetic field lines with fluid, the second term describes the α -effect, and the last term determines diffusion and dissipation of the field.

For describing the average magnetic field, following Parker (1955), we choose a local coordinate system, xyz , where z represents the radial coordinate, axis y is the azimuthal coordinate and axis x coincides with co-latitude. Effects of sphericity are not included in this model. Hence, the vector of the mean field, $\langle \mathbf{B} \rangle$, can be represented as

$$\langle \mathbf{B} \rangle = B(x, y) \mathbf{e}_y + \nabla \times [A(x, y) \mathbf{e}_y], \quad (2.3)$$

where $B(x, y)$ is the toroidal component of magnetic field, $A(x, y)$ is the vector-potential of the poloidal field. Assuming that $\langle \mathbf{v} \rangle = v_y(x) \mathbf{e}_y$ (rotational component), we can write the dynamical system describing Parker's model of the α -dynamo (Parker 1955) in the standard form:

$$\frac{\partial A}{\partial t} = \alpha B + \eta \nabla^2 A, \quad \frac{\partial B}{\partial t} = G \frac{\partial A}{\partial x} + \eta \nabla^2 B, \quad (2.4)$$

where $G = \partial \langle v_y \rangle / \partial z$ is the rotational shear.

Assuming that the coefficients are constants and seeking a solution of the model in the form $(A, B_y) \sim (A_0, B_0) \exp[i(kx - \omega t)]$, we find the well-known result that a pure periodic solution exists if $D = \alpha G / (\eta^2 k^3) = 2$, where D is the so-called six ‘‘dynamo number.’’ The solutions grow in time for $D > 2$, and decay for $D < 2$.

For periodic solutions toroidal and poloidal field components vary in time in a sinusoidal fashion, which is clearly different from the observed, asymmetric profile of the solar cycle (Fig. 1b). As shown by Kitiashvili & Kosovichev (2009), in the one-mode

approximation the classical Parker's dynamo model gives only periodic oscillatory solutions, and therefore cannot explain the observed variations of the sunspot number in the solar cycles. For creating chaotic variations of the magnetic field in the low-mode approximation it is necessary to add to the Parker's model a third equation describing variations of the magnetic helicity and its interaction with the large-scale magnetic field (Kleeorin & Ruzmaikin 1982; Kleeorin *et al.* 1995).

2.2. The Kleeorin-Ruzmaikin model

For modeling the solar cycle we choose the formulation of Kleeorin & Ruzmaikin (1982), which is based on the idea of magnetic helicity conservation, and has reasonable agreement with the observational data of solar magnetic fields (Kleeorin *et al.* 2003; Sokoloff 2007). Due to the fact that the kinetic helicity makes the magnetic field small-scaled, the back influence on the turbulent fluid motions can restrict the unlimited growth of the magnetic field. In the mean-field approach the magnetic helicity is separated into large- and small-scale components. Because of the conservation of the total helicity, a growth of the large-scale magnetic helicity due to the dynamo action is compensated by the growth of the small-scale helicity of opposite sign (Sokoloff 2007). Thus, small- and large-scale magnetic fields grow together and are mirror-asymmetrical. This means that the condition of magnetic helicity conservation is, perhaps, more severe for restricting the dynamo action than the condition of the energy conservation.

The turbulent helicity can be divided into two parts: hydrodynamic and magnetic: $\alpha = \alpha_h + \alpha_m$. The kinetic helicity, α_h , describes helical turbulent fluid motions; the magnetic helicity, α_m , determines the order of twisted magnetic field lines:

$$\alpha_h = -\tau \langle \mathbf{u} \cdot (\nabla \times \mathbf{u}) \rangle / 3, \quad \alpha_m = \tau \langle \mathbf{b} \cdot (\nabla \times \mathbf{b}) \rangle / (12\pi\rho), \quad (2.5)$$

where τ is the lifetime of turbulent eddies, ρ is density.

It is convenient to define the influence of the magnetic helicity on magnetic field using spectral density $\bar{\chi}$ (Kleeorin & Ruzmaikin 1982)

$$\bar{\chi} \equiv \langle \mathbf{a} \cdot \mathbf{b} \rangle, \quad (2.6)$$

where \mathbf{a} is the fluctuating part of the magnetic field vector-potential, \mathbf{A} .

To derive an equation for the averaged helicity density we multiply the basic induction equation (2.1) written without the differential rotation term by the fluctuating part of the vector potential, \mathbf{a} ; and also multiply the equation for the vector-potential

$$\frac{\partial \mathbf{A}}{\partial t} = \mathbf{v} \times \mathbf{B} - \eta_m \nabla \times \nabla \times \mathbf{A}, \quad (2.7)$$

by the fluctuating part of magnetic field \mathbf{b} . Using the averaging of the sum of Eqs. (2.1) and (2.7), and taking into account that $\mathbf{b} = \nabla \times \mathbf{a}$, after some transformations we obtain the following expression for the helicity density (Kleeorin & Ruzmaikin 1982; Kitiashvili & Kosovichev 2009)

$$\frac{\partial \bar{\chi}}{\partial t} = \left\langle \mathbf{a} \cdot \frac{\partial \mathbf{b}}{\partial t} + \mathbf{b} \cdot \frac{\partial \mathbf{a}}{\partial t} \right\rangle = -2 \langle [\mathbf{v} \times \mathbf{b}] \cdot \langle \mathbf{B} \rangle \rangle - 2\eta_m \langle \mathbf{b} \cdot \nabla \times \mathbf{b} \rangle. \quad (2.8)$$

Two terms, $\langle \Delta[\mathbf{a} \times [\mathbf{v} \times \langle \mathbf{B} \rangle]] \rangle$ and $\langle \Delta[\mathbf{a} \times [\mathbf{v} \times \mathbf{b}]] \rangle$, disappear as a result of volume averaging. Using the mean-field electrodynamics approximation and retaining only the first two terms for the mean electric field (Moffatt 1978)

$$\varepsilon \equiv \langle \mathbf{v} \times \mathbf{b} \rangle \cong \alpha \langle \mathbf{B} \rangle - \eta (\nabla \times \langle \mathbf{B} \rangle), \quad (2.9)$$

we obtain

$$\frac{\partial \bar{\chi}}{\partial t} = 2 \left(\eta \langle \mathbf{B} \rangle \cdot (\nabla \times \langle \mathbf{B} \rangle) - \alpha \langle \mathbf{B} \rangle^2 - \eta_m \langle \mathbf{b} \cdot \nabla \times \mathbf{b} \rangle \right). \quad (2.10)$$

Then, the expression for variations of the magnetic helicity, α_m , in terms of the mean magnetic field is the following (Kleeorin & Ruzmaikin 1982):

$$\frac{\partial \alpha_m}{\partial t} = \frac{Q}{2\pi\rho} \left[\langle \mathbf{B} \rangle \cdot (\nabla \times \langle \mathbf{B} \rangle) - \frac{\alpha}{\eta} \langle \mathbf{B} \rangle^2 \right] - \frac{\alpha_m}{T}, \quad (2.11)$$

where coefficient $Q \sim 0.1$, T is the characteristic time for magnetic diffusion. Equation (2.11) is written for the case of uniform turbulent diffusion, and when the magnetic Reynolds number is large, $\eta \approx \eta_t$.

For further analysis of the Kleeorin-Ruzmaikin model we transform Eqs. (2.4) and (2.11) in a non-linear dynamical system in non-dimensional variables. Following the approach of Weiss *et al.* (1984) we average the system of Eqs. (2.4) and (2.11) in a vertical layer to eliminate z -dependence of A and B and consider a single Fourier mode propagating in the x -direction assuming $A = A(t)e^{ikx}$, $B = B(t)e^{ikx}$; then we get the following system of equations

$$\begin{aligned} \frac{dA}{dt} &= \alpha B - \eta k^2 A, & \frac{dB}{dt} &= ikGA - \eta k^2 B, \\ \frac{d\alpha_m}{dt} &= -\frac{\alpha_m}{T} - \frac{Q}{2\pi\rho} \left[-ABk^2 + \frac{\alpha}{\eta} (B^2 - k^2 A^2) \right]. \end{aligned} \quad (2.12)$$

This transformation allows us to investigate more easily various non-linear regimes, from periodic to chaotic, and obtain relationships of the basic properties, such as the cycle growth and decay times, duration and amplitude. Note that the formulation and the interpretation of solutions of the simplified system are not straightforward because it does not adequately describes non-linear coupling of the spatial harmonics. For simplicity we retain only the second harmonic ($k = 2$), which has the largest growth rate among the antisymmetric solutions.

To relate the dynamo model solutions to the observations we used Bracewell's definition (1953, 1988) of the sunspot number in the form $W \sim B(t)^{3/2}$, where $B(t)$ is the toroidal magnetic field component. We note that the solutions of the dynamical system are qualitatively similar for the different harmonics. Nevertheless, we choose the parameters, which correspond to the solar situation.

Making the following substitutions: $A = A_0 \hat{A}$, $B = B_0 \hat{B}$, $t = T_0 \hat{t}$, $k = \hat{k}/r$ (r is a layer radius), $T_0 = 1/(k^2\eta)$ and $\alpha_m = \alpha_0 \hat{\alpha}_m$, and taking into account that $A_0 = B_0 \eta k/G$, we obtain:

$$\begin{aligned} \frac{d\hat{A}}{d\hat{t}} &= \hat{D}\hat{B} - \hat{A}, & \frac{d\hat{B}}{d\hat{t}} &= i\hat{A} - \hat{B}, \\ \frac{d\hat{\alpha}_m}{d\hat{t}} &= -\nu\hat{\alpha}_m + \left[\hat{A}\hat{B} - \hat{D} \left(\hat{B}^2 - \lambda\hat{A}^2 \right) \right], \end{aligned} \quad (2.13)$$

where $\hat{D} = D_0 \hat{\alpha}$ and $\hat{\alpha} = \hat{\alpha}_h + \hat{\alpha}_m$ are the non-dimensional dynamo number and total helicity, $D_0 = \alpha_0 G r^3 / \eta^2$, $\alpha_0 = 2Qk v_A^2 / G$, v_A is the Alfvén speed, ν is the ratio of the characteristic times of turbulent and magnetic diffusion (Kleeorin & Ruzmaikin 1982) and $\lambda = (k^2 \eta / G)^2 = \text{Rm}^{-2}$, and Rm is the magnetic Reynolds number.

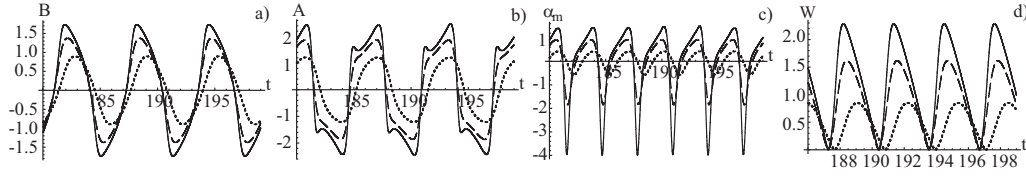


FIGURE 2. Variations of the magnetic field for the middle convective zone $\alpha_h D_0 = -2$: $\nu = 1.28$, $\alpha_h = 2.439$, $D_0 = -0.82$ for different initial conditions: $B_0 = 4i$, $A_0 = -0.01i$ (dotted curve), $B_0 = 4i$, $A_0 = -i$ (dashed curve) and $B_0 = 1 + 4i$, $A_0 = -i$ (solid curve): a) toroidal component, B ; b) vector-potential, A , of the poloidal magnetic field; c) magnetic helicity variations, α_m ; d) evolution of the model sunspot number, W .

2.3. Periodic and chaotic solutions

In order to estimate the range of parameters of the Kleorin-Ruzmaikin model Eq. (2.12) and for modeling the solar cycle, we use the standard model of the interior structure rotation of the Sun for the top, bottom and middle areas of the convective zone (Schou *et al.* 1998). The key parameter of the model is the dynamo number $D = D_0 \alpha_h$, because its magnitude determines behavior of the magnetic field, which depends on the rotational velocity and magnetic field strength. According to Kitiashvili & Kosovichev (2009) for the Kleorin-Ruzmaikin model, given by Eqs (2.12), the linear instability condition is also $|D| \equiv |\alpha_h D_0| > 2$. However, in this case the profile of the periodic solutions is not sinusoidal, and depends on the initial conditions, A_0 and B_0 . For higher initial values the amplitude of the non-linear oscillations in the stationary state is higher. However, the shapes of the oscillation profiles are similar.

Figure 2 illustrates solutions for the model of Kleorin-Ruzmaikin, and the corresponding variations of the sunspot number for different initial conditions. As mentioned, different initial values for magnetic field components A_0 and B_0 lead to very similar profiles. In high amplitude cases, dual peaks may appear in the variations of the vector potential, A , of the poloidal field. The evolution of the magnetic helicity shows a relatively slow growth followed by a sharp decay (Kitiashvili & Kosovichev 2009). The helicity has maxima when the toroidal field is zero. In these calculations the value of parameter ν , which describes damping rate of magnetic helicity and depends on the turbulence spectrum and the dissipation through helicity fluxes, is of the order of unity. Finally, the variations of the sunspot number, W , with the amplitude increase are characterized by higher peaks and shorter rising times (see Fig. 2d). Note that in the sunspot number profile we can recognize the well-known general properties of the sunspot number profile with a rapid growth at the beginning of the cycle and a slow decrease after the maximum.

With the increasing of $|\alpha_h D_0|$ ($|\alpha_h D_0| > 2$) the profile of magnetic field variations continue to deform and can become unstable with very steep variations of the magnetic field. The solution can be stable again if we enhance the back reaction by increasing the quenching parameter. We use the following quenching formula for the kinetic part of helicity, α_h , Kleorin *et al.* (1995) $\alpha = \alpha_h / (1 + \xi B^2) + \alpha_m$. Thus we can always obtain periodic solutions for sufficiently strong ξ .

The transition from periodic to chaotic solutions occurs when the dynamo number, $|\alpha_h D_0|$, increases above a certain value. In the transition regime the cycle amplitude becomes modulated: it slowly increases with time, and then suddenly and very sharply declines, and then starts growing again (Kitiashvili & Kosovichev 2009).

In the case of significant deviations from the condition of linear stability, the solutions become chaotic for all variables of the dynamical system. Figure 3 shows an example of

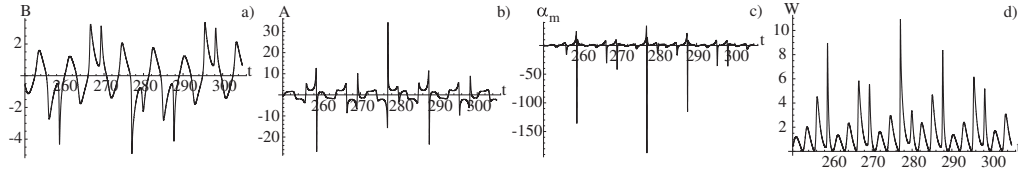


FIGURE 3. Example of the chaotic solution for the middle convective zone parameters: a) toroidal component of magnetic field B , b) vector-potential, A , c) magnetic helicity variations α_m and d) model sunspot number W .

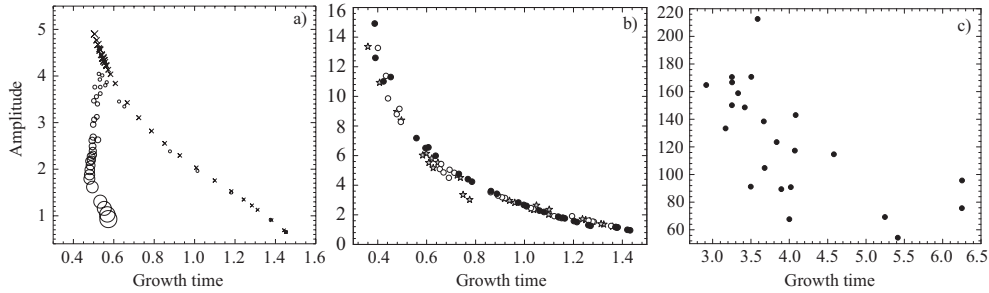


FIGURE 4. Relationships between the amplitude of the model sunspot number and the growth time for a) periodic solutions: the circles show a sequence for a fixed value of the kinetic helicity, $\alpha_h = 2.44$, and the dynamo number varying from -7 to -0.82 ; the crosses show the case of fixed $D_0 = -0.82$ and α_h varying from 2.44 to 3 (the size of crosses and circles is proportional to the corresponding values of $|D_0|$ and α_h); b) chaotic solutions for $D_0 = -0.82$ and $\alpha_h = 2.8$ (black circles), $\alpha_h = 3$ (empty circles) and $\alpha_h = 3.2$ (stars); and c) for the real solar cycles.

chaotic variations for the middle convective zone parameters: $\nu = 1.28$, $\lambda = 1.23 \times 10^{-6}$, $D_0 = -0.82$, $\alpha_h = 3.2$, $\xi = 3.9 \times 10^{-3}$ for the magnetic field components, the magnetic helicity and the sunspot number parameter. In the chaotic solutions, the peaks of the toroidal magnetic field, B (Fig. 3a) strongly correlate with the peaks of the vector-potential, A , and the magnetic helicity, α_m , (Fig. 3b, c). The growth of the toroidal field also leads to strengthening of the poloidal field and strong fluctuations of the magnetic helicity.

Now we can see from Figs. 2d and 3d that the profiles of the model sunspot number variations qualitatively describe the mean profile of the solar cycles. The next important characteristic of the solar cycles is the relationship between the amplitude and the growth time. Figure 4 shows this relationship for some periodical solutions (panel a), four chaotic solutions (panel b) and properties for the real 23 solar cycles (panel c). The time scales are non-dimensional. Figure 4c shows the observed amplitude-growth time properties of the solar cycles of 1755 – 2007. Thus, all three panels demonstrate that the growth time is shorter for stronger cycles.

3. Data assimilation methods

In the previous section we obtained a solution for the dynamical system in one-mode approximation, which qualitatively reproduces the basic properties of the solar cycle. In this section we try to adapt the periodic model solution and sunspots number series using data assimilation methods.

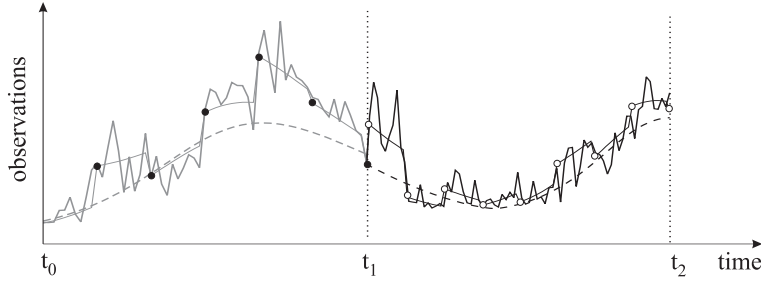


FIGURE 5. Scheme of the data assimilation procedure. Dashed curves show exact solutions of a model, thin solid curves describe the first correction of a model according to observations, thick curves are the best estimate of an observable system state. Gray and black colors indicate estimations for past and forecast states. Black and empty circles mean real and simulated observations, respectively.

3.1. Basic formulation

The main goal of any model is an accurate description of properties of a system in the past and present times, and the prediction of its future behavior. However, a model is usually constructed with some approximations and assumptions, and contains uncertainties. Therefore, it cannot describe the true condition of a system. On the other hand, observational data, d , also include errors, ϵ , which are often difficult to estimate. Data assimilation methods such as the Kalman Filter (Kalman 1960) allow us, with the help of an already constructed model and observational data, to determine the initial state of the model that is in agreement with a set of observations, and obtain a forecast of future observations and an error estimate (Evensen 2007; Kitiashvili 2008). For instance, in our case we know from observations the sunspot number (with some errors) and want to estimate the state of the solar magnetic fields, described by a dynamo model.

In generally, if the state, ψ , of a system can be described by a dynamical model $d\psi/dt = g(\psi, t) + q$, with initial conditions $\psi_0 = \Psi_0 + p$, where $g(\psi, t)$ is a non-linear vector-function, q and p are the errors of the model and in the initial conditions. Then, the system forecast is $\psi^f = \psi^t + \phi$, where ψ^t is the true system state, and ϕ is the forecast error. The relationship between the true state and the observational data is given by a relation $d = M[\psi] + \epsilon$, where d is a vector of measurements, $M[\psi]$ is a measurement functional.

For a realization of the data assimilation procedure in the case of non-linear dynamics, it is convenient to use the Ensemble Kalman Filter (EnKF) method (Evensen 1994, 2007). The main difference of the EnKF from the standard Kalman Filter is in using an ensemble of possible states of a system, which can be generated by Monte Carlo simulations. If we have an ensemble of measurements $d_j = d + \epsilon_j$ with errors ϵ_j (where $j = 1, \dots, N$), then we can define the covariance matrix of the measurement errors $C_{\epsilon\epsilon}^e = \overline{\epsilon\epsilon^T}$, where the overbar means the ensemble averaged value, and superscript T indicates transposition. Using a model we always can describe future states of a system, ψ^f . However, errors in the model, initial conditions and measurements do not allow the model result be consistent with observations. To take into account this deviation, we consider a covariance matrix of the first-guess estimates (our forecast related only to model calculations): $(C_{\psi\psi}^e)^f = (\psi^f - \overline{\psi^f})(\psi^f - \overline{\psi^f})^T$. Note that the covariance error matrix is calculated for every ensemble element. Then, the estimate of the system state is given by:

$$\psi^a = \psi^f + K (d - M\psi^f), \quad (3.1)$$

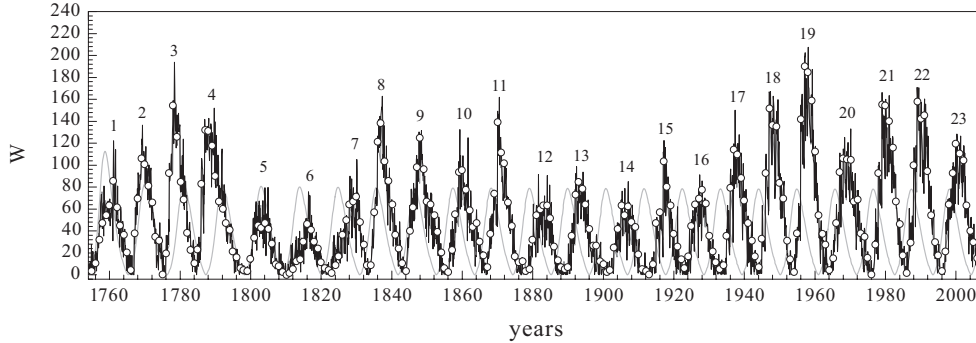


FIGURE 6. Results of assimilation of the annual sunspot number data (circles) into the dynamo model. The gray curve shows the reference solution (without assimilation analysis), and the black curve shows the best EnKF estimate of the sunspot number variations, obtained from the data and the dynamo model.

where $K = (C_{\psi\psi}^e)^f M^T (M(C_{\psi\psi}^e)^f M^T + C_{\epsilon\epsilon}^e)^{-1}$, is the so-called Kalman gain (Kalman 1960; Evensen 2007). The covariance error matrix of the best estimate is calculated as $(C_{\psi\psi}^e)^a = (\psi^a - \bar{\psi}^a)(\psi^a - \bar{\psi}^a)^T = (I - K_e M) (C_{\psi\psi}^e)^f$. We can use the last best estimate obtained with the available observational data as the initial conditions and make the next forecast step. At the forecast step, we calculate a reference solution of the model, according to the new initial conditions, then simulate measurements by adding errors to the model and to the initial conditions. Finally we obtain a new best estimate of the system state, which is our forecast. A new set of observations allows us to redefine the previous model state and make a correction for the predicted state.

3.2. Implementation of the data assimilation method

For the assimilation of the sunspot data into the dynamo model, we select a class of periodic solutions which correspond to parameters of the middle convective zone and describe the typical behavior of the sunspot number variations (Fig. 2d). The implementation of the EnKF method consists of three steps (Kitiashvili & Kosovichev 2008): preparation of the observational data for analysis, correction of the model solution according to observations, and prediction.

Step 1: Preparation of the observational data. Following Bracewell (1953, 1988), we transform the annually averaged sunspot number for the period of 1856 – 2007 into the toroidal field values using the relationship $B \sim W^{2/3}$ while alternating the sign of B . We also select the initial conditions of the model such that the reference solution coincides with the beginning of the first cycle in our series, cycle 10, which started in 1856. We do not consider the previous solar cycles because of the uncertainties in the early sunspot number measurements. Then we normalize the toroidal field in the model in such a way that the model amplitude of B is equal to the mean toroidal field calculated from the sunspot number. In addition, we normalize the model time scale assuming that the period of the model corresponds to the typical solar cycle duration of 11 years.

Step 2: Assimilation for the past system state. Unfortunately we do not have observations of the magnetic helicity, and the toroidal and poloidal components of the magnetic field. Therefore, in the first approximation, we generate observational data as random values around the reference solution with a standard deviation of $\sim 12\%$, which was chosen to roughly reproduce the observed variations of the sunspot number. Then, we

calculate the covariance error matrixes of the observations, $C_{\epsilon\epsilon}^e$, and the forecast, $(C_{\psi\psi}^e)^f$. After combining the observation and model error covariances in the Kalman gain, K , we obtain the best estimate for the evolution of the system, ψ^a from Eq. (3.1) (Fig. 5, first half). Figure 6 shows the result of assimilation of the sunspot data into the dynamo model: the best EnKF estimate (black curve), the initial model (gray curve) and the actual sunspot data (circles).

Step 3: Prediction. Obtain a prediction of the next solar cycle, we determine the initial conditions from the best estimated solution for the previous cycle in terms of the amplitude and phase to continue the model calculations. Then after receiving the reference solution with the new initial conditions, we simulate future observational data by adding random noise and repeat the analysis (Fig. 5, right). This provides the best EnKF estimate of the future state of the system (forecast).

3.3. Reproducing and predicting observational data by the Ensemble Kalman Filter

The described analysis has been tested by calculating predictions of previous cycles. Figure 7 (a-h) shows examples of the EnKF method implementation for forecasting the sunspot number of cycles 16–23. For these forecasts, we first obtain the best estimated solutions using the observational data prior to these cycles. We then compute the model solution (black dashed curves) according to the initial conditions of the time of the last measurement and simulate a new set observation by adding random noise. Then, we obtain the EnKF estimates using the simulated observations, which give us the prediction (Fig. 7, black curves). These experiments show that this approach can provide reasonable forecast of the strength of the next solar cycles. However, there are significant discrepancies. For instance, the strength of cycle 16 is over-estimated, and the strength of cycle 19 is under-estimated. The main uncertainties are caused by inaccuracies in determining the time of the end of the previous cycle from the sunspot number data, and by the incompleteness of the model and insufficiency of the sunspot number data. In particular, we found the forecast is inaccurate when the sunspot number change significantly from the value of the previous cycle (Kitiashvili & Kosovichev 2008). Also, our forecast experiments show a strong dependence on the phase relation between the reference model solution and the observations. The phase difference appears due to the constant period of the model solution. Curiously, when the model phase is ahead of the solar cycle phase, adding a data point at the start of the cycle substantially improves the forecast. However, when the model phase lags, this does not happen. This effect is taken into account by correcting the phase of a reference solution that it is slightly ahead of the solar cycle phase.

The same analysis scheme is applied for predicting of the next solar cycle 24. According to this result, solar cycle 24 will be weaker than the previous cycle by approximately 30%. To test the stability of this prediction we used two other sets of initial conditions in 2008 and obtained close results (Fig. 7i).

4. Results and discussion

We have presented a numerical analysis of simple dynamical models describing the non-linear behavior of two dynamo models, the classical Parker’s dynamo model with the standard α -quenching and the model of Kleeorin & Ruzmaikin (1982), which describes the evolution of the magnetic helicity based on the balance between the large-scale and turbulent magnetic helicities, shows the existence of non-linear periodic and chaotic solutions. Using a low-order dynamical system approach we examine the influence of the

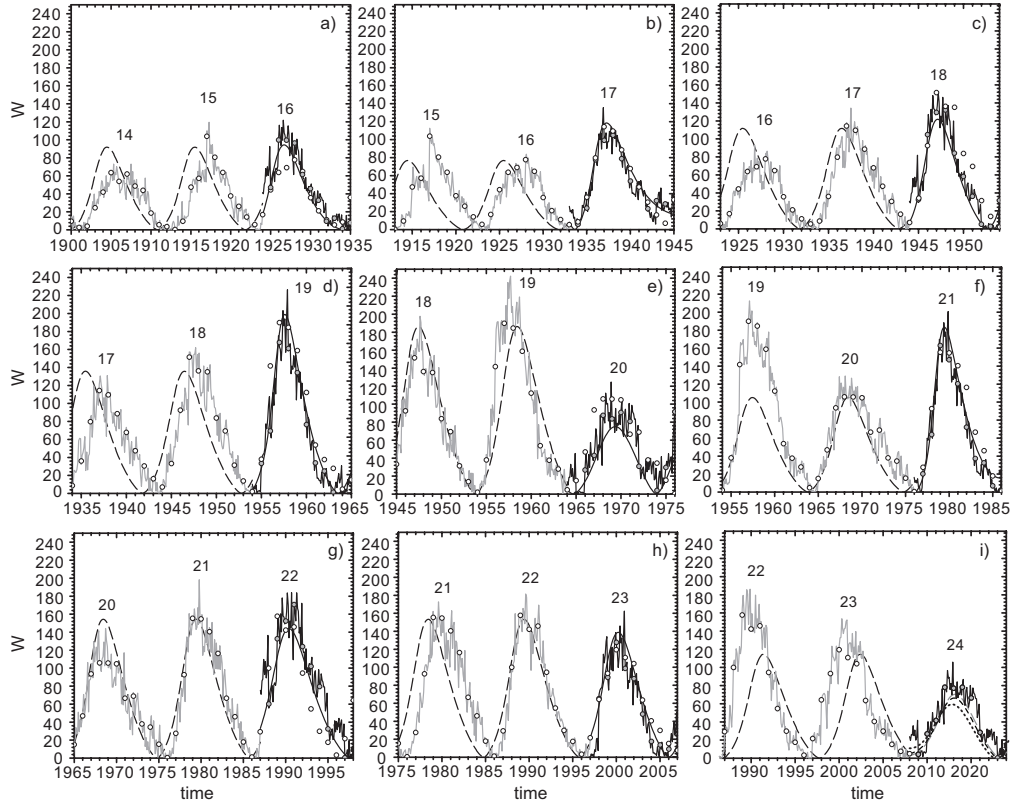


FIGURE 7. Predictions for solar cycles 16–24. Black dashed curves show the time model reference solution. Gray curves show the best estimate of the sunspot number using the observational data (empty circles) and the model, for the previous cycles. Black curves show the prediction results. In panel i) the model solution is shown for three different estimates of the sunspot number for 2008: 3 (gray dashed curve), 5 (black dashed curve) and 10 (dots).

kinetic and magnetic helicities on the non-linear fluctuations of the dynamo-generated magnetic field in the conditions of the solar plasma, and compare these with the sunspot number variations observed during the solar 11-year cycles.

The analysis of the Kleorin-Ruzmaikin model showed the existence of non-linear periodic and chaotic solutions for conditions of the solar convective zone. For this model we obtained profiles of the sunspot number variations, which qualitatively reproduce the typical profile of the solar cycles.

The results of assimilation of the annual sunspot number data into the solar dynamo model and the prediction of the previous solar cycles (Fig. 7) demonstrate a new method of forecasting the solar activity cycles. Using the EnKF method and a simple dynamo model, we obtained reasonable predictions usually for the first half of sunspot cycles with an error of $\sim 8\text{--}12\%$, and in some cases also for the declining phase of the cycles. This method predicts a weak solar cycle 24 with a maximum of the smoothed annual sunspot number of approximately 80. It is interesting to note that the simulations show that the previous cycle does not finish in 2007 as was expected, but still continues into 2008. According to the prediction, the maximum of the next cycle will be reached approximately in 2013.

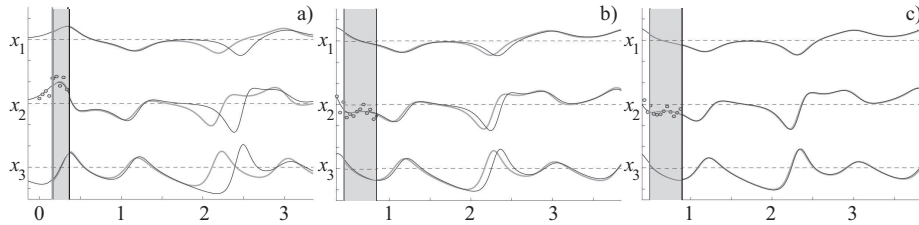


FIGURE 8. Example of implementation of the EnVE algorithm to the Lorenz system for all three states with true model solution. Black curve shows exact solution of the model, gray line represents model forecast and dots is measurements. a) Initially, the estimate is fairly poor, as seen by the quickly diverging forecast; b) as the estimate is improved, the variational window (shadow area) width expands, helping to further reduce the error in the forecast; and c) the estimate converges accurately to the global minimum (Bewley *et al.* 2008).

The application of the data assimilation method, EnKF, for modeling and predicting solar cycles shows the power of this approach and encourages further development. It also reveals significant uncertainties in the model and the data. Among these are the uncertainties in the determination of the start of a solar cycle from the sunspot number series (in particular, when the cycles overlap), leading to the uncertainty in the phase relation between the model solution and the data. Also, there are significant uncertainties in the relationship between the sunspot number data and the physical properties of the solar magnetic field, in the absence of magnetic field and helicity data, and, of course, in the dynamo model. Our conclusion is that for more robust and accurate predictions of solar cycles, the information contained in the sunspot number data is insufficient.

5. Future work

For further development we plan to apply the data assimilation methods to more complete 2-D dynamo models, which describe the latitudinal distribution of the solar magnetic field, and use the magnetograph data available for the past three cycles.

In addition, we would like to use alternative, more advanced methods. Therefore we plan to apply the hybrid Ensemble Variational Estimation (EnVE) method (Cessna *et al.* 2008; Bewley *et al.* 2008). This method is a combination of the EnKF and 4DVar methods. The EnVE algorithm is initialized by using the traditional EnKF scheme up to the time of the most current measurement. This provides the current, best ensemble estimate together with the corresponding implicit statistics. The mean estimate is found by taking the average of all the ensemble members. In addition, a variational iteration similar to 4DVar is set up to allow for a multiscale optimization. For forecasting applications, the most important estimate is the one at the most recent measurement time, because it is used as an initial condition for the forecasting calculations. It is especially important for correct predictions of solar cycles to correctly determine the time of the solar minima, particularly for early cycles when observations were irregular and less accurate. This problem can be partially solved by using the EnVE method, because the method redefines previous states of a system by back integration in time. Previously this method was tested by Bewley *et al.* (2008) for a Lorenz model (Fig. 8). The results have shown a good prediction for the chaotic system. Thus, we hope for success in the implementation of the EnVE method for solar dynamo models.

Acknowledgements

This work was partially supported by the International Space Science Institute (Bern).

REFERENCES

- BRACEWELL, R. N. 1953 The sunspots number series. *Nature* **171**, 649–650.
- BRACEWELL, R. N. 1988 Three-halves law in sunspot cycle shape. *Mon. Not. R. Astr. Soc* **230**, 535–550.
- BRANDENBURG, A. & SUBRAMANIAN, K. 2005 Astrophysical magnetic fields and non-linear dynamo theory. *Physics Reports* **417**, 1–209.
- BEWLEY, T., CESSNA, J. & COLBURN, C. 2008 EnVE: a consistent hybrid ensemble/variational estimation strategy for multiscale uncertain systems. *Tellus*, in press.
- CESSNA, J., COLBURN, C. & BEWLEY, T. 2008 EnVE: a new estimation algorithm for weather forecasting and flow control. *Proc. of 4th Low Control Conference*, 23–26 June, 2008, Seattle, Washington, AIAA 2008-4314, 6pp.
- EVENSEN, G. 1994 Sequential data assimilation with a nonlinear quasi-geostrophic model using Monte Carlo methods to forecast error statistics. *J. Geophys. Res.* **99**(C5), 10143–10162.
- EVENSEN, G. 2007 *Data assimilation. The Ensemble Kalman Filter*. Berlin, Germany, Springer.
- IVANOVA, T.S. & RUZMAIKIN, A.A. 1977 A nonlinear magnetohydrodynamic model of the solar dynamo. *Sov. Astron.* **21**, 479–485.
- KALMAN, R. E. 1960 A new approach to linear filtering and prediction problems. *J. Basic Engineering* **82**(series D), 35–45.
- KITIASHVILI, I. 2008 Application of data assimilation methods to non-linear solar dynamo models. *ASP Conf. Series* **383**, 255–263.
- KITIASHVILI, I. N. & KOSOVICHEV, A. G. 2008 Application of data assimilation method for predicting solar cycles. *Astrophys. Journal Letters* **688**, L49–L52.
- KITIASHVILI, I. N. & KOSOVICHEV, A. G. 2009 Nonlinear dynamical modeling of solar cycles using dynamo formulation with turbulent magnetic helicity. *Geophys. Astrophys. Fluid Dyn.* **103**, 16pp., in press.
- KLEEORIN, N. I. & RUZMAIKIN, A. A. 1982 Dynamics of the mean turbulent helicity in magnetic field. *Magnetohydrodynamics* **18**, 116–122.
- KRAUSE, F. & RÄDLER, K.-H. 1980 *Mean-field magnetohydrodynamics and dynamo theory*. Oxford, UK, Pergamon Press.
- MOFFATT, H. K. 1978 *Magnetic field generation in electrically conducting fluids*. New York: Cambridge Univ. Press.
- KLEEORIN, N., KUZANYAN, K., MOSS, D., ROGACHEVSKII, I., SOKOLOFF, D. & ZHANG, H. 2003 Magnetic helicity evolution during the solar activity cycle: observations and dynamo theory. *Astron. Astrophys.* **409**, 1097–1105.
- KLEEORIN, N., ROGACHEVSKII, I. & RUZMAIKIN, A. 1995 Magnitude of the dynamo-generated magnetic field in solar-type convective zones. *Astron. Astrophys.* **297**, 159–167.
- PARKER, E. N. 1955 Hydromagnetic dynamo models. *Astrophys. J.* **122**, 293–314.
- SCHOU, J. et al. 1998 Helioseismic studies of differential rotation in the solar envelope by the solar oscillations investigation using the Michelson Doppler Imager. *Astrophys. J.* **505**, 390–417.

- SOKOLOFF, D. 2007 Astrophysical dynamos and magnetic helicity conservation. *Plasma Phys. Control. Fusion* **49**, B447–B452.
- WEISS, N. O., CATTANEO, F. & JONES, C. A. 1984 Periodic and aperiodic dynamo waves. *Geophys. Astrophys. Fluid Dyn.* **30**, 305–341.